Hybrid GaAs-Nanowire–Carbon-Nanotube Flexible Photovoltaics

Parsian K. Mohseni, Gregor Lawson, Alex Adronov, and Ray R. LaPierre, *Member, IEEE*

***Abstract*—A simple method is described for the preparation of carbon nanotube (CNT) composite films containing Au nanoparticles, which act as adatom collection agents promoting the growth of core–shell p-n junction GaAs nanowires (NW), according to the vapor–liquid–solid mechanism. This approach for composite film formation requires no covalent modification of the CNTs. GaAs NWs obtained are randomly aligned with respect to the CNT substrate in a densely packed arrangement. Nanohybrid films, incorporating coaxial GaAs NWs as the active, light-harvesting medium are used in the fabrication of photovoltaic cells, exhibiting conversion efficiencies up to 0.32%. Doping experiments confirm that conduction is not dominated by Schottky barriers at contact interfaces. The NW/CNT solar cells are shown to retain function following bending up to a curve radius of 12.5 mm, illustrating the potential of these novel materials in flexible device applications.**

***Index Terms*—Carbon nanotubes (CNTs), molecular beam epitaxy, photovoltaic (PV) cell fabrication, semiconductor nanowires (NWs).**

I. Introduction

ONE-DIMENSIONAL structures play a unique role in the landscape of nanometer-scale science and engineering. In this realm, semiconductor nanowires (NWs) and carbon nanotubes (CNTs) have attracted interest by demonstrating quantum mechanical phenomena and integration within a new generation of electronic and photonic devices [1]. Furthermore, the combination of semiconducting NWs or CNTs with more mature functional materials, such as thin films and polymers, has demonstrated enhanced functionality and improved device performance [2]–[6].

Of particular significance is the solar energy conversion potential possessed by semiconductor NWs. This stems from a variety of factors including their inherent light-trapping capabilities, as NW ensembles allow for improved optical absorption, in comparison to their thin film or textured-surface counterparts [7]. There is particular interest in coaxial p-n junction NWs where, for example, a p-doped core is surrounded by an n-doped shell. With this geometry, charge carriers are efficiently separated by the coaxial p-n junction across the NW diameter, d, which can be smaller than the carrier diffusion length, thereby promoting high-efficiency collection of photogenerated carriers [8]. Recently, numerous efforts have demonstrated the photovoltaic (PV) capabilities of semiconductor NWs, based on Si [9]–[12], III–V [13], [14], and II–VI [15]–[17] materials. As NWs can easily be integrated with a variety of functional substrates, fabrication of mechanically flexible, NW-based optoelectronic devices has attracted considerable attention [18] and remains a matter of continual importance.

We recently reported that single-walled CNT (SWNT) composite films decorated by Au nanoparticles can be employed as substrates for the assembly of III–V semiconductor NWs, [19] according to the vapor–liquid–solid (VLS) mechanism [20]–[22]. In this prior work, thin films of poly(ethyleneimine) functionalized CNTs, prepared using the vacuum filtration method [23]–[25], were decorated with Au nanoparticles by *in situ* reduction of $HAuCl_4$ under mild conditions [26]. These SWNT–Au composite films were subsequently used as substrates for the growth of GaAs NWs in a gas-source molecular beam epitaxy (GS-MBE) system. Following this procedure, randomly aligned NWs were obtained in high density across the entire surface of the SWNT substrates. Characterization of these NWs, using TEM and microphotoluminescence, revealed them to be of high purity and optical quality. This work, therefore, represented the development of a novel nanohybrid material that combines the optoelectronic properties of GaAs NWs with the impressive flexibility and conductivity of CNT films and, as such, displays apparent potential in the development of flexible, lightweight electronic devices such as PVs, LEDs, and sensors.

In this paper, we demonstrate that these hybrid nanomaterials can indeed be used in the fabrication of PV cells, wherein coaxial p-n junction GaAs NWs act as the active medium for energy conversion, while the underlying CNT films simultaneously serve as robust, flexible electrodes. Additionally, we outline a simplified method for the preparation of SWNT–Au composite substrates that requires no covalent modification of CNTs, thereby greatly reducing the time required for composite film fabrication and also improving the retention of the CNTs electrical properties.

II. Experimental

A. SWNT–Au Composite Film Preparation

Single-walled CNTs were purchased from Carbon Nanotechnologies, Inc. (Houston, TX). SWNTs were produced by the

Manuscript received March 4, 2010; revised April 7, 2010; accepted April 7, 2010. Date of publication June 21, 2010; date of current version August 5, 2011. This work was supported by the Natural Sciences and Engineering Research Council of Canada, the Ontario Centers of Excellence, the Canada Foundation for Innovation, and the Ontario Innovation Trust.

P. K. Mohseni and R. R. LaPierre are with the Department of Engineering Physics and the Center for Emerging Device Technologies, McMaster University, Hamilton, ON L8 S 4L7, Canada (e-mail: pkmohseni@mcmaster.ca; lapierr@mcmaster.ca).

G. Lawson and A. Adronov are with the Department of Chemistry and the Brockhouse Institute for Materials Research, McMaster University, Hamilton, ON L8 S 4L7, Canada (e-mail: lawsong@mcmaster.ca; adronov@mcmaster.ca).

Color versions of one or more of the figures in this paper are available online at http://ieeexplore.ieee.org.

Digital Object Identifier 10.1109/JSTQE.2010.2048097

HiPco process and were used as received. Nanotube samples were dispersed in solvent using a Branson 1510 bath sonicator. Nanotube dispersions were centrifuged using a Beckman Coulter Allegra X-22 Centrifuge.

The Au nanoparticles were prepared using the well-established citrate-reduction method [27]–[29], which results in near monodisperse particles. Deposition of Au nanoparticles was achieved by filtration of a dilute nanoparticle solution through a thin film of unmodified SWNTs, prepared by vacuum filtration of a SWNT dispersion in aqueous surfactant solution. CNT thin films, such as those prepared in this study, resemble a random finely interpenetrating network of nanotube bundles. The porous microstructure of these films makes them ideal candidates for use as high-efficiency fibrous filtration membranes. Several groups have investigated the potential of CNTs in separation and filtration applications [30]–[37]. Although much of this work has focused upon the use of aligned CNT arrays, Lipowicz and coworkers reported the effective removal of fine airborne particulate, having dimension as small as 50 nm, using thin films composed solely of randomly aligned multiwalled CNTs [32].

The current approach for the fabrication of SWNT–Au substrates offers several advantages over the previously reported *in situ* reduction method [26]. Covalent modification of CNTs, which was necessary in our previous work, results in conversion of numerous carbon atoms within the framework of the CNTs to sp^3 hybridization, disrupting the π system of the CNTs and significantly diminishing their electrical conductivity [38]. It is expected that the use of unfunctionalized SWNTs, in our modified procedure, will reduce the likelihood that the structure and electronic properties of the CNTs will be compromised during film fabrication. As the modified approach requires few synthetic steps, the time required for the preparation of each composite film is greatly reduced. In addition, the current procedure allows for fine control over the size and polydispersity of Au nanoparticles deposited on the nanotube surface.

Following fabrication, composite films were cut into small sections having dimensions of approximately 5×10 mm, removed from the filtration membranes and transferred [23], Au nanoparticle side up, to copper substrates. Copper was arbitrarily chosen as a rigid, conductive, and GS-MBE-compatible support material to which the CNT films could easily be transferred for subsequent NW growth or later removed. These samples were then thermally annealed at 550 °C for 10 min in nitrogen ambient, ensuring the removal of volatile organic matter, which could potentially contaminate the MBE chamber during NW growth.

B. Growth of GaAs NWs

The GS-MBE system used for NW growths was equipped with a solid elemental effusion cell, for the supply of Ga monomers, and a hydride (AsH_3) gas cracker operating at 950 °C, for the supply of As_2 dimers. Prior to the commencement of the growth sequence, a degas procedure (15 min, 300 °C) was performed, followed by an inductively coupled hydrogen plasma treatment (10 min, 550 °C), under an As_2 overpressure. This is a standard sample cleaning procedure whose impact on CNT substrates requires further investigation. This procedure was adopted to provide for NW growth conditions that were consistent with those used in [13] and [19] for comparison purposes. At a growth temperature of 550 °C, NW growth was instigated by opening the shutter of the Ga cell. All growths were kept at a constant V/III flux ratio of 1.5 and nominal GaAs growth rate of 1 μm/h. Upon the completion of growth, prompted by the termination of Ga flux, the samples were cooled under an As_2 overpressure.

For the purposes of investigations presented in this study, two NW groups were grown on CNT composite sheets, henceforth referred to as groups A and B. Group A NWs were designed to contain a p-n junction within a coaxial architecture, based upon diffusion-limited nucleation on the lateral NW facets, wherein an n-GaAs core segment was doped with Te, while a p-GaAs shell was doped with Be. Each segment of the group A NWs was grown for a duration of 15 min, resulting in a total growth period of 30 min. Group B NWs, in contrast, were entirely n-type doped with Te, also over a growth period of 30 min, yielding n-GaAs NWs. Nominal dopant concentrations were maintained at 4×10^{18} cm^{-3} and 5×10^{18} cm^{-3}, for Te and Be levels, respectively, based upon previous calibrations of epitaxial films on GaAs (100) substrates. The group A NWs were primarily used to assess the PV potential of such NW–CNT hybrid materials, while the group B NWs were employed in investigations into the nature of the PV response and the conduction pathways between the NWs and their underlying CNT substrates.

Additionally, a third growth was carried out, referred to as group C, wherein a planar p-n junction was incorporated into a thin film deposited upon a CNT composite film containing no Au nanoparticles. This control sample was grown with the intention of mimicking the structure of the planar GaAs film deposited during the growth, and situated adjacent to the bases, of the group A and B NWs. The group C samples were prepared consisting of a 150-nm-thick Be-doped GaAs layer overlaying a 150-nm-thick Te-doped GaAs layer. Identical CNT film processing (surface decoration of Au nanoparticles, notwithstanding) and GS-MBE growth parameters including temperature, nominal growth rate, III/V flux ratio, and nominal doping concentration were employed during thin film depositions and NW growths. Thus, the GaAs film of sample C was designed to duplicate the properties of the planar film concurrently deposited during NW growth.

C. Solar Cell Fabrication and Contacting Procedure

To prevent potential short circuit pathways between top contacts and the bottom CNT electrode, a previously reported processing method was employed [13], [19]. Starting with as-grown samples, SiO_x layers, approximately 1300 Å in thickness, were deposited through plasma-enhanced chemical vapor deposition (PE-CVD), to conformally coat the NWs (and the exposed surface of the GaAs films growing between the NWs) atop the CNT substrate. Subsequent spin coating of S-1808 photoresist was carried out to encapsulate the oxide-coated NWs and GaAs film. Next, an O_2-plasma-reactive-ion-etching (RIE) treatment

(60 s) allowed for the removal of a thin photoresist film, thereby exposing the tips of the oxide-coated NWs.

The oxide-coated tips were then chemically etched in a buffered-hydrofluoric acid solution and the remaining photoresist layer was removed in an acetone bath lift-off procedure. At this stage, the NW bases and adjacently situated GaAs film remained encapsulated by the previously deposited SiO_x layer, while NW tips were exposed as the sole semiconductor surface upon which electrical contacts could be deposited.

Two different conductive materials were employed as top contact layers in this study. For experiments aimed toward investigations into PV behavior, a 1000-Å-thick transparent conductive film of indium tin oxide (ITO) was deposited via sputter coating. For direct comparison of the conductive behavior of group A and B NWs, where optimal Ohmic contacts are required, opaque contacts were deposited on the processed samples. In this case, the commonly used Ti/Pt/Au and Ni/Ge/Au layers were deposited on groups A and B samples, respectively, via electron-beam evaporation. In all cases, the depositions were made through shadow masks allowing for contact dots roughly 800 μm in diameter. Inspection of plan view SEM images (not shown) indicated that each contact dot yielded the ensemble contribution of approximately 1.5×10^6 individual NWs. After the deposition of ITO or opaque contacts, the samples were subjected to a rapid thermal annealing (RTA) treatment (30 s, 400 °C) for Ohmic contact formation.

SEM imaging was performed during pregrowth inspection of Au-decorated CNT films, during analysis of the orientation and morphology of as-grown NWs, and during each stage of the device fabrication procedure. The SEM imaging was performed using a JEOL JSM-7000 F SEM, equipped with a Schottky-type field-emission gun filament. In addition, inspection of the CNT films were performed by focused ion beam (FIB) cross sectioning using a Zeiss NVision SII Cross-Beam instrument.

D. Current–Voltage Characterization Under Dark and Illuminated Conditions

The current–voltage characteristics of the various samples were evaluated using a Keithley 2400 source meter. A Newport 96000 solar simulator with an A.M. 1.5 G filter yielding an incident power of roughly 2.6 Sun was used as the illumination source in measuring PV response. Conversion efficiencies and fill factors were calculated according to standard techniques [39].

III. Results and Discussion

Fig. 1 shows planar SEM images of SWNT–Au composite film samples (A) before and (B) after thermal annealing at 550 °C for 10 min in nitrogen ambient. Prior to the thermal anneal, Au nanoparticles have an average diameter of 30 ± 5 nm. This value increases to 38 ± 6 nm following the annealing procedure, as a result of the migration and coalescence of a small fraction of Au nanoparticles at elevated temperatures. It can, however, be seen, from the SEM images in Fig. 1, that large-scale aggregation of Au nanoparticles does not occur during this process. The density of Au nanoparticles upon the surface of annealed composite films, which was also determined using SEM, ranged between 20 and 86 nanoparticles per 1 μm^2, with an average density of 50 nanoparticles per 1 μm^2.

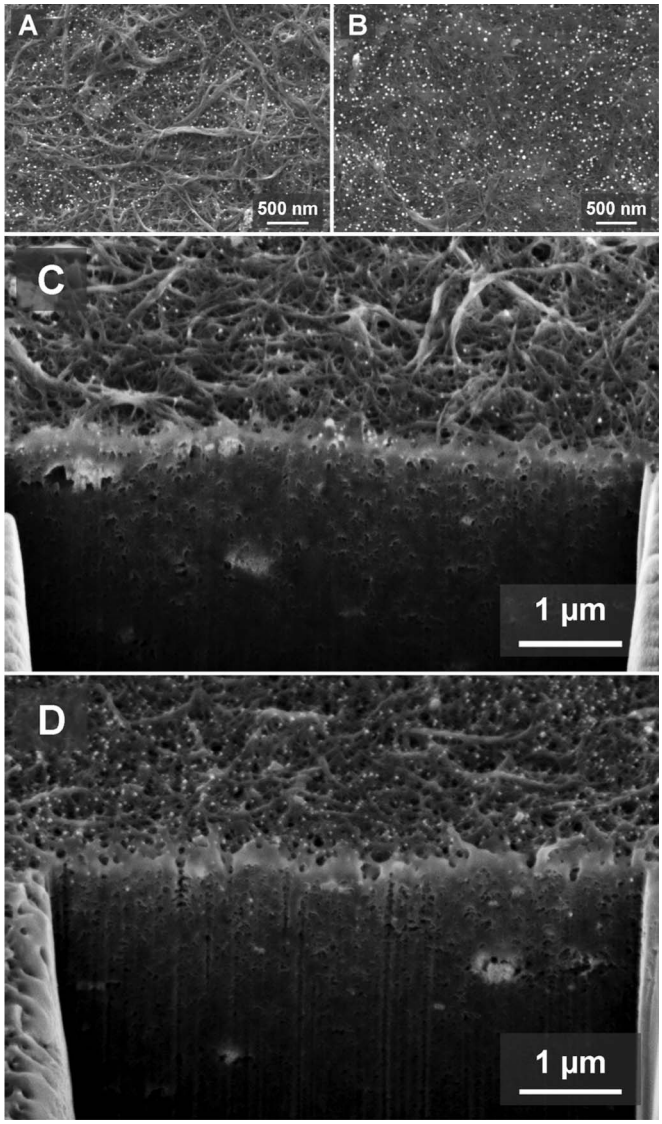

Fig. 1. Planar SEM images (secondary electrons) of a SWNT–Au thin film, (A) before and (B) after RTA at 550 °C for 10 min under nitrogen, and tilted SEM cross-sectional images of trenches milled within SWNT–Au films (C) before and (D) after the same annealing procedure.

Cross-sectional images of these films were obtained after FIB milling. A trench cut within a SWNT–Au composite film, which has not undergone thermal annealing, is shown in Fig. 1(C). In this secondary electron image, Au nanoparticles are observed to be located predominantly upon the film's surface. Some Au nanoparticles can also be seen in low density within the structure of the nanotube film. The presence of Au nanoparticles within the film is not unexpected, given the film's porous microstructure and the dimensions of Au nanoparticles used in this study. In addition to Au nanoparticles, clusters of iron were also detected, embedded within the nanotube film. These clusters, which appear as regions of bright contrast in Fig. 1(C) and (D)

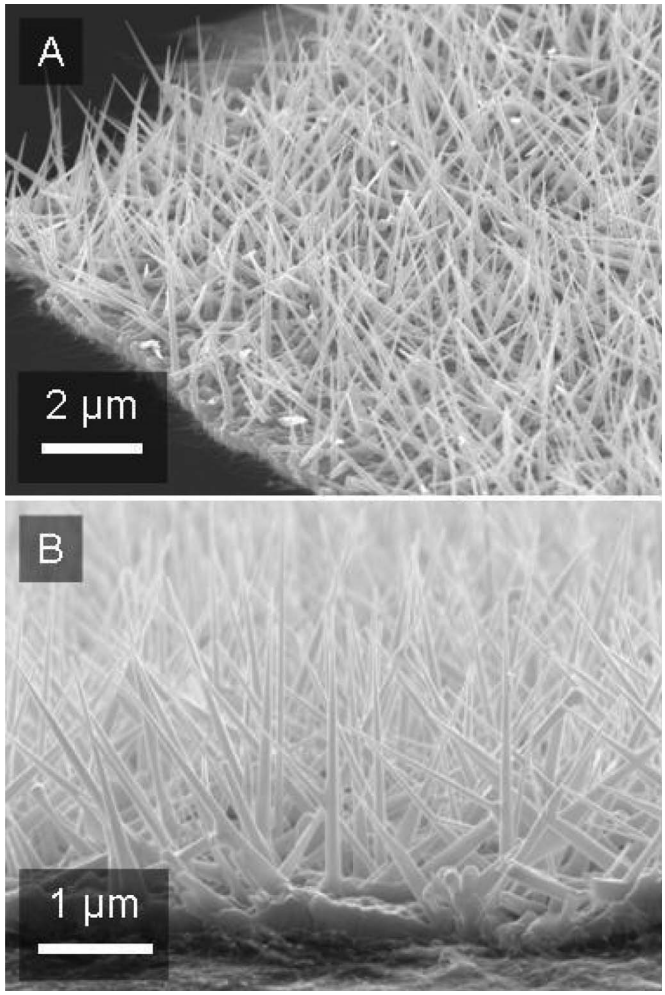

Fig. 2. 45° (A) tilted view and (B) cross-sectional SEM images of as-grown group A NW samples. Densely packed NWs are grown at various orientations with a highly tapered morphology. Similar results were obtained from group B NW samples.

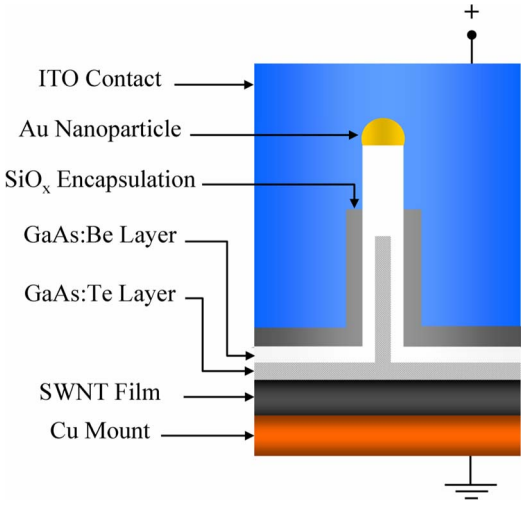

Fig. 3. Schematic representation of group A NW solar cell, showing biasing conditions. The NW bases and planar GaAs film are electrically isolated from the ITO top contact. The CNT substrate simultaneously serves as the growth surface and backside contact.

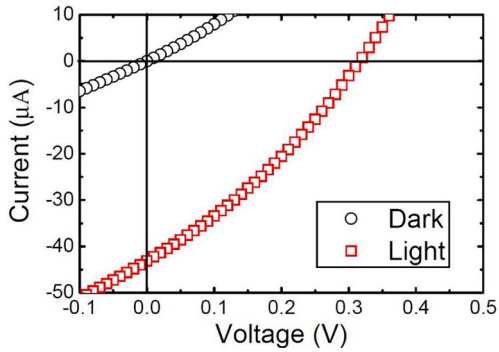

Fig. 4. Current–voltage curve of group A NWs, with ITO top contacts, under dark and 2.6 Sun illumination. Group B NWs demonstrated no such photoresponse.

having dimensions on the scale of 10 s to 100 s of nanometers, are impurities present in the commercially purchased nanotube sample used in this study (Fe catalyst from SWNT synthesis). Fig. 1(D) illustrates a similar trench produced by FIB milling of a sample that has been annealed at 550 °C. From these images, it was determined that the distribution of Au nanoparticles throughout our SWNT–Au composite films is not significantly altered by the annealing.

SEM images of group A NWs, shown in Fig. 2, showed dense NW growth with no preferred NW orientation (similar results were obtained from group B NWs). The random alignment of NWs relative to the substrate surface was previously attributed to the random manner in which SWNT bundles comprising the underlying film are situated [19]. As determined from sample sets of over 100 single specimens, the NWs have an average full-width at half-length diameter of roughly 100 nm and heights up to 3.5 μm. The highly tapered morphology is a trademark of diffusion-limited sidewall growth and is anticipated for GS-MBE growths under the growth conditions employed [19], [40].

As outlined in the Section II, solar cell fabrication was carried out through a process designed to effectively exploit NWs as the active, energy conversion medium. A schematic representation of the final device structure, showing a single NW for clarity, is depicted in Fig. 3. In light of recent reports on the inhomogeneity of dopant profiles in semiconductor NWs [41], [42] and the anticipated incongruity in dopant incorporation between the (1 0 0) surface of the doping calibration sample and the (1 1 1) surfaces of the NWs, the degree of uniformity in the dopant distributions within the samples discussed here remains a matter of further scrutiny. Nonetheless, a clear distinction can be made between group A NWs (those containing a p-n junction in a core–shell homostructure) and group B NWs (those intentionally highly n-doped).

Upon fabrication, the PV response of the NW solar cells was measured. Fig. 4 shows the fourth quadrant current–voltage characteristics of an ensemble of ITO contacted group A NWs, under dark (black, circular data points) and 2.6 Sun illumination (red, square data points) conditions. A clear PV response is evident, attributed to the sum contribution of all contacted

NWs in the contact area. Although varying efficiency values were measured from different contact dots, likely due to different numbers of NWs contacted by each dot and small growth temperature variances across the sample leading to slightly dissimilar NW structures, each contact dot exhibited reproducible efficiencies. The optimal efficiency curve, shown in Fig. 4, was characterized by a short-circuit current, $I_{\rm SC} = 43.1\ \mu$A (equivalently, $J_{\rm SC} = 8.57$ mA/cm^2 for the 800 μm diameter contact dot), an open-circuit voltage, $V_{\rm OC} = 0.32$ V, a maximum power, $P_{\rm max} = 42.3\ \mu$W, a fill factor of 30.8%, and a maximum conversion efficiency of 0.32%. No such conversion response was evident in group B NWs (n-doped NWs) contacted with the transparent conductive oxide layer, indicating that the PV effect was due to the p-n junctions in group A NWs.

In comparison, previously reported ensemble contacted NW-based solar cells [9], [10], [13], [14], [43], [44] have demonstrated maximum measured conversion efficiencies ranging between 0.1% and 4.5%. For example, coaxial p-n Si NW cells grown by the vapor–liquid–solid (VLS) process gave an efficiency of 0.1% on stainless steel substrates [9]. Si NW cells on glass substrates formed by wet electroless etching yielded efficiencies of 4.4% [10]. Coaxial p-n Si NW cells grown by the VLS process gave an efficiency of <1% on Si substrates [43]. An efficiency of 0.1% was reported for VLS-grown Si NWs on multicrystalline Si thin films on glass [44]. A single GaAs NW cell was recently reported with an efficiency of 4.5% [14]. The design most comparable to that of the current study is detailed in [13], where a PV effect was measured from vertically oriented GaAs NWs grown on n-GaAs (1 1 1) B substrates with a photoconversion efficiency of 0.83%. The lower efficiency values achieved on our CNT films, in comparison to the vertically oriented NWs, may be attributed to two main features. First, growth on CNT films results in NWs grown at a variety of dissimilar angles with respect to the film surface. During the contacting procedure, NWs oriented at more acute angles relative to the CNT film are likely to remain encapsulated by the photoresist layer used during the device processing. Consequently, only the NWs grown at relatively large angles to the substrate will be contacted, meaning that only an undetermined fraction of all NWs will have conductive pathways allowing for their photogenerated holes to be collected. Thus, the total contribution toward the quoted conversion efficiency is not necessarily a reflection of all NWs in the ensemble, but rather only the ones in contact with the ITO film.

Based on previous analysis [19], we believe that an intimate, atomically abrupt interface exists between the CNT film and overlaying GaAs NWs. The distinct Au-nanoparticle decoration technique used in this study is not expected to dramatically alter the atomic nature of the NW/CNT interface. However, in view of the fact that the CNT film in this study serves not only as the substrate, but also as the electrical contact for the emitter layer of the solar cell, the conduction pathway at this junction requires further consideration. In fact, the second factor contributing to the noted efficiency degradation is the additional series resistance as a result of a barrier at the n-GaAs/CNT interface. Fig. 5(A) shows a 1-D band diagram, with respect to axial distance along a single group A NW, assuming a NW length of 2 μm, and

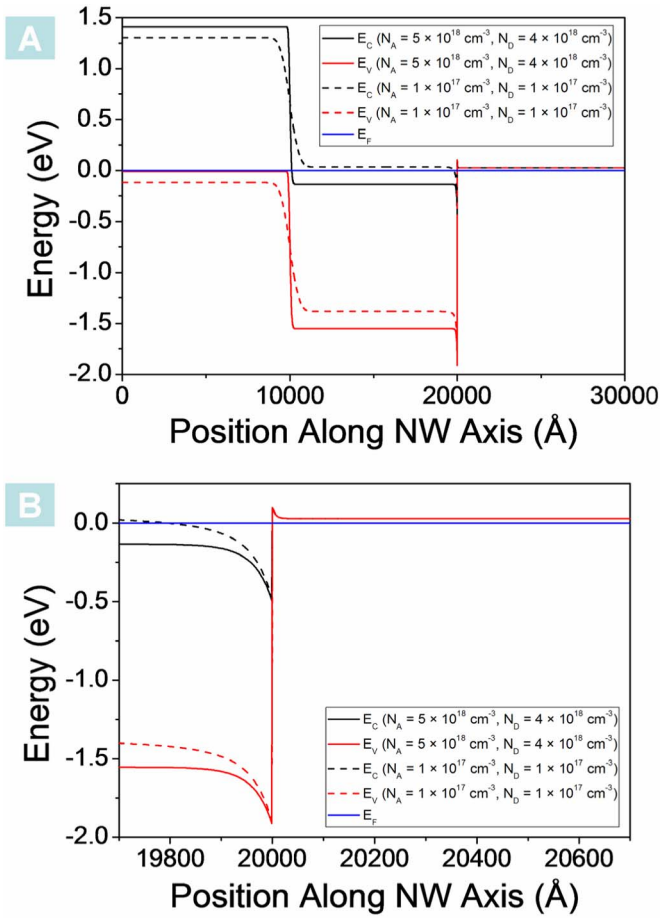

Fig. 5. (A) One-dimensional energy band diagram as a function of axial position along a single, 2-μm-long, group A NW. The p-type segment, n-type segment, and CNT film are shown from left to right. Black and red lines denote the conduction and valence bands, respectively. The solid lines represent the band energies according to nominal doping levels quoted in the paper, while the dashed lines represent energies at a reduced dopant concentration of 1×10^{17} cm^{-3}. The solid blue line represents the Fermi energy, $E_{\rm F}$. (B) Magnified view of (A) at the n-GaAs/CNT interface, showing the presence of a small energy barrier.

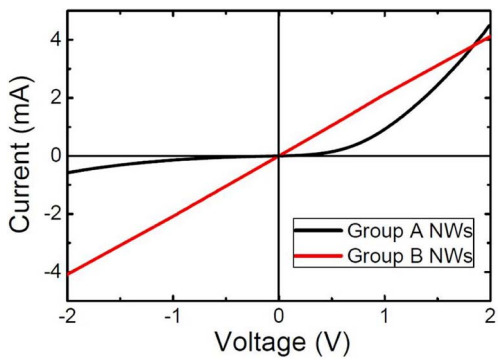

Fig. 6. Comparison of current–voltage characteristics of group A (black curve) and group B (red line) NWs, contacted with opaque Ti/Pt/Au and Ni/Ge/Au layers, respectively. Rectification is exhibited by the p-n junction NWs while Ohmic behavior is exhibited by the heavily n-doped NWs.

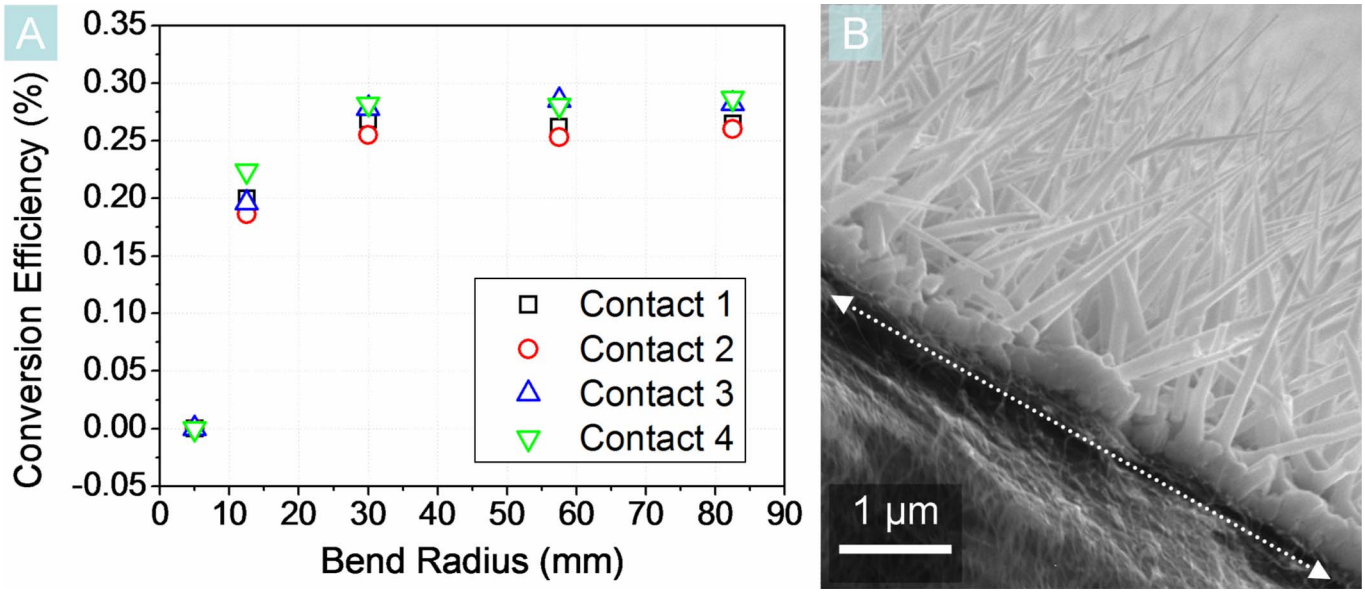

Fig. 7. (A) Measured conversion efficiency as a function of device flexure at various bend radii (curvature increasing from right to left). A 25% decrease in efficiency is observed at a radius of 12.5 mm. Additional bending beyond this point results in device failure. (B) SEM image of sample curved beyond the critical radius of failure. The white, dotted line indicates the fracture plane where the GaAs NWs are separated from the CNT substrate.

derived using a SWNT film work function of 4.5 eV [45]. The band diagram was calculated using a 1-D Poisson–Schrödinger equation solver, based upon a finite-difference method, and is described in [46]. Here, the p-type GaAs segment is shown on the left side, the n-type GaAs segment in the middle, and the CNT substrate on the right. Conduction band and valence band energies are depicted by black and red lines, respectively, while the Fermi level is shown as a solid blue line. The solid lines represent the band structure anticipated from layers with the nominal doping concentrations, discussed previously. The dotted lines, on the other hand, represent the energy bands that would result from acceptor and donor concentrations of 1×10^{17} cm^{-3}. This doping concentration is over one order of magnitude less than the quoted nominal level, and is shown as an expected lower limit of dopant incorporation within the NW core, according to Perea *et al.* [41]. Fig. 5(B) shows a magnified view of the energy barrier present at the n-GaAs/CNT interface. The collection of photogenerated electrons is, therefore, preceded by either carrier tunneling from the n-GaAs NW segment to the underlying CNT film or by thermionic emission, dependant upon the concentration of dopants incorporated within the NW bulk.

We previously showed that the current–voltage characteristics of a collection of group-A-type NWs exhibited asymmetric rectifications, and had attributed this diode-type behavior directly to the p-n junctions incorporated within the NW structures [19]. Characterization of electrical junctions within composite films has subsequently been conducted to determine the electrical quality of the junctions and whether ideal current flow is inhibited by Schottky effects at the interfaces. In Fig. 6, the current–voltage characteristics of group A and B NWs, contacted by opaque contacts, are compared. As seen here, this study shows a similar current rectification from the group A NWs, while group B NWs exhibit a linear behavior over the same voltage range. Similarly, group B NWs contacted with ITO also exhibited linear current–voltage characteristics. We present this distinguishing feature (rectifying behavior of p-n junction NWs in sample A versus Ohmic behavior of n-doped NWs in sample B) as the defining trademark of the desired dopant activation in our NWs, and evidence that the diode-type behavior previously presented is not merely a manifestation of Schottky barriers at the n-GaAs/CNT interface. The low forward-bias currents evident in the group A curve may be attributed to the partial depletion of the NWs. Furthermore, the aforementioned doping levels and NW density under each contact dot should exhibit resistance values on the order of tens of milliohms, while the measured resistance is on the order of 100 Ω. This discrepancy may be ascribed to contact resistances suffered during the measurement process, as well as the effect of the GaAs/CNT interface.

The influence of the planar GaAs layer, deposited alongside the NWs, upon the observed PV effect was also studied. As a lateral p-n junction exists in this layer, it is important to distinguish whether this element contributes to the measured conversion efficiency. To this end, the group C control samples were prepared with total film thickness chosen to mimic the average thickness of the planar GaAs layer in group A NW samples, as determined through cross-sectional transmission-electron-microscopy analysis. This film was subsequently contacted with ITO dots, equal to the thickness of that situated atop the processed group A NWs (as revealed through SEM inspection), such that optical absorption would be comparable between the control and test samples. Under the illuminated solar cell testing conditions described above, the group C control sample reproducibly exhibited an open-circuit voltage of $V_{\rm OC} < 25$ μV and a short-circuit current of $I_{\rm SC} < 20$ nA, from all contact dots tested, representing negligible PV behavior. The lack of a PV response in the control sample is chiefly attributed to a high concentration of grain boundaries in the polycrystalline GaAs film, which act as

sites for the recombination of any photogenerated electron–hole pairs. Thus, the planar GaAs layer makes no PV contribution and the energy conversion efficiency observed in group A samples can be attributed to the p-n junction NWs grown atop the CNT composite films.

Similarly, the potential for photocurrent generation resulting from a Schottky contact at the ITO/p-GaAs NW interface is not expected. Havard *et al.* [47] have shown that, under the annealing conditions employed in this study, Ohmic behavior is anticipated at the ITO/p-GaAs NW interface. Furthermore, based on the work functions of ITO (4.6–5 eV) and p-GaAs (∼5.5 eV), the current flow anticipated from a Schottky ITO/p-GaAs interface would occur in a direction opposite to the observed current flow as expected from the NW p-n junction.

A final point of added interest is the degree of flexibility and operable range of the group A NW solar cells. The conversion efficiency of the fabricated devices was measured while being subjected to mechanical bending at various radii of curvature. Fig. 7(A) plots measured efficiency as a function of bend radius between 82.5 and 5 mm, for four particular contact dots. As the curvature of the devices increased (see from right to left in Fig. 7), it was noted that conversion efficiencies were stable to a bend radius of 30 mm. Increasing curvature, to a bend radius of 12.5 mm, resulted in the degradation of efficiency by approximately 25%. Further flexure beyond this point led to the onset of full device failure. Based on SEM analysis of samples intentionally curved past the critical radius of failure [see Fig. 7(B)], we attribute the breakdown mechanism to fracture of the polycrystalline GaAs film and its detachment, along with the NWs, from the conductive substrate. Thus, beyond the critical curvature, the photogenerated carriers are no longer effectively collected.

IV. Conclusion

In summary, a modified regime for the fabrication of Au-nanoparticle-decorated SWNT films has been presented that requires no covalent functionalization of the CNTs. Coaxial p-n GaAs NWs were grown upon these flexible, conductive substrates, and subsequently, employed in the fabrication of PV cells. Thus, the light harvesting potential of GaAs NWs on flexible CNT films has been demonstrated. The devices demonstrate PV behavior when curved, up to a bend radius of 12.5 mm. Further curvature leads to failure due to mechanical fracture and detachment of the GaAs film deposited simultaneously between the NWs. We predict that the vacuum filtration method for SWNT composite film fabrication outlined in this study will be applicable to any nanomaterial having dimensions that enable their capture and immobilization upon the surface of SWNT membranes. We therefore envision that this scheme can lend itself to the deposition of a variety of inorganic nanoparticles, and consequently, to the incorporation of NWs composed of a wide range of semiconducting materials, and containing sophisticated heterostructures. This approach may be employed for the production of next generation flexible optoelectronic devices.

Acknowledgment

The authors gratefully acknowledge Dr. B. Robinson for GS-MBE growths, Dr. H. Bi for assistance during the final fabrication stage, and Dr. F. Gonzaga for assistance in the preparation of Au nanoparticle samples.

References

[1] M. Law, J. Goldberger, and P. D. Yang, "Semiconductor nanowires and nanotubes," *Annu. Rev. Mater. Res.*, vol. 34, pp. 83–122, 2004.

[2] T. A. G. Eberlein, R. Jones, J. P. Goss, and P. R. Briddon, "Doping of graphene: Density functional calculations of charge transfer between GaAs and carbon nanostructures," *Phys. Rev. B*, vol. 78, pp. 045403-1–045403-5, 2008.

[3] S. Y. Ju, A. Facchetti, Y. Xuan, J. Liu, F. Ishikawa, P. D. Ye, C. W. Zhou, T. J. Marks, and D. B. Janes, "Fabrication of fully transparent nanowire transistors for transparent and flexible electronics," *Nat. Nanotechnol.*, vol. 2, pp. 378–384, 2007.

[4] K. Lee, Z. Wu, Z. Chen, F. Ren, S. J. Pearton, and A. G. Rinzler, "Single wall carbon nanotubes for p-type ohmic contacts to GaN light-emitting diodes," *Nano Lett.*, vol. 4, pp. 911–914, 2004.

[5] M. C. McAlpine, R. S. Friedman, S. Jin, K. H. Lin, W. U. Wang, and C. M. Lieber, "High-performance nanowire electronics and photonics on glass and plastic substrates," *Nano Lett.*, vol. 3, pp. 1531–1535, 2003.

[6] R. C. Tenent, T. M. Barnes, J. D. Bergeson, A. J. Ferguson, B. To, L. M. Gedvilas, M. J. Heben, and J. L. Blackburn, "Ultrasmooth, largearea, high-uniformity, conductive transparent single-walled-carbonnanotube films for photovoltaics produced by ultrasonic spraying," *Adv. Mater.*, vol. 21, pp. 1–7, 2009.

[7] O. L. Muskens, J. G. Rivas, R. E. Algra, E. P. A. M. Bakkers, and A. Lagendijk, "Design of light scattering in nanowire materials for photovoltaic applications," *Nano Lett.*, vol. 8, pp. 2638–2642, 2008.

[8] B. M. Kayes, H. A. Atwater, and N. S. Lewis, "Comparison of the device physics principles of planar and radial p-n junction nanorod solar cells," *J. Appl. Phys.*, vol. 97, pp. 114302–114311, 2005.

[9] L. Tsakalakos, J. Balch, J. Fronheiser, B. A. Korevaar, O. Sulima, and J. Rand, "Silicon nanowire solar cells," *Appl. Phys. Lett.*, vol. 91, pp. 233117-1–233117-3, 2007.

[10] V. Sivakov, G. Andra, A. Gawlik, A. Berger, J. Plentz, F. Falk, and S. H. Christiansen, "Silicon nanowire-based solar cells on glass: Synthesis, optical properties, and cell parameters," *Nano Lett.*, vol. 9, pp. 1549–1554, 2009.

[11] Y. J. Dong, B. Z. Tian, T. J. Kempa, and C. M. Lieber, "Coaxial group III-nitride nanowire photovoltaics," *Nano Lett.*, vol. 9, pp. 2183–2187, 2009.

[12] B. Z. Tian, X. L. Zheng, T. J. Kempa, Y. Fang, N. F. Yu, G. H. Yu, J. L. Huang, and C. M. Lieber, "Coaxial silicon nanowires as solar cells and nanoelectronic power sources," *Nature*, vol. 449, pp. 885–U888, 2007.

[13] J. A. Czaban, D. A. Thompson, and R. R. LaPierre, "GaAs core-shell nanowires for photovoltaic applications," *Nano Lett.*, vol. 9, pp. 148–154, 2009.

[14] C. Colombo, M. Heiss, M. Gratzel, and A. F. I. Morral, "Gallium arsenide p-i-n radial structures for photovoltaic applications," *Appl. Phys. Lett.*, vol. 94, pp. 173108-1–173108-3, 2009.

[15] C. Xu, X. Wang, and Z. L. Wang, "Nanowire structured hybrid cell for concurrently scavenging solar and mechanical energies," *J. Amer. Chem. Soc.*, vol. 131, pp. 5866–5872, 2009.

[16] B. D. Yuhas and P. D. Yang, "Nanowire-based all-oxide solar cells," *J. Amer. Chem. Soc.*, vol. 131, pp. 3756–3761, 2009.

[17] M. Law, L. E. Greene, J. C. Johnson, R. Saykally, and P. D. Yang, "Nanowire dye-sensitized solar cells," *Nat. Mater.*, vol. 4, pp. 455–459, 2005.

[18] A. Nadarajah, R. C. Word, J. Meiss, and R. Konenkamp, "Flexible inorganic nanowire light-emitting diode," *Nano Lett.*, vol. 8, pp. 534–537, 2008.

[19] P. K. Mohseni, G. Lawson, C. Couteau, G. Weihs, A. Adronov, and R. R. LaPierre, "Growth and characterization of GaAs nanowires on carbon nanotube composite films: Toward flexible nanodevices," *Nano Lett.*, vol. 8, pp. 4075–4080, 2008.

[20] R. S. Wagner and W. C. Ellis, "Vapor-Liquid-Solid mechanism of single crystal growth," *Appl. Phys. Lett.*, vol. 4, pp. 89–90, 1964.

[21] V. G. Dubrovskii, N. V. Sibirev, G. E. Cirlin, J. C. Harmand, and V. M. Ustinov, "Theoretical analysis of the vapor-liquid-solid mechanism of nanowire growth during molecular beam epitaxy," *Phys. Rev. E*, vol. 73, pp. 021603–021610, 2006.
[22] H. J. Fan, P. Werner, and M. Zacharias, "Semiconductor nanowires: From self-organization to patterned growth," *Small*, vol. 2, pp. 700–717, 2006.
[23] Z. C. Wu, Z. H. Chen, X. Du, J. M. Logan, J. Sippel, M. Nikolou, K. Kamaras, J. R. Reynolds, D. B. Tanner, A. F. Hebard, and A. G. Rinzler, "Transparent, conductive carbon nanotube films," *Science*, vol. 305, pp. 1273–1276, 2004.
[24] F. Hennrich, S. Lebedkin, S. Malik, J. Tracy, M. Barczewski, H. Rosner, and M. Kappes, "Preparation, characterization and applications of free-standing single walled carbon nanotube thin films," *Phys. Chem. Chem. Phys.*, vol. 4, pp. 2273–2277, 2002.
[25] L. Hu, D. S. Hecht, and G. Gruner, "Percolation in transparent and conducting carbon nanotube networks," *Nano Lett.*, vol. 4, pp. 2513–2517, 2004.
[26] G. Lawson, F. Gonzaga, J. Huang, G. de Silveira, M. A. Brook, and A. Adronov, "Au-carbon nanotube composites from self-reduction of Au^{3+} upon poly(ethylene imine) functionalized SWNT thin films," *J. Mater. Chem.*, vol. 18, pp. 1694–1702, 2008.
[27] J. Turkevich, J. Hillier, and P. C. Stevenson, "A study of the nucleation and growth processes in the synthesis of colloidal gold," *Discuss. Faraday. Soc.*, vol. 11, p. 55, 1951.
[28] J. Kimling, M. Maier, B. Okenve, V. Kotaidis, H. Ballot, and A. Plech, "Turkevich method for gold nanoparticle synthesis revisited," *J. Phys. Chem. B*, vol. 110, pp. 15700–15707, 2006.
[29] X. H. Ji, X. N. Song, J. Li, Y. B. Bai, W. S. Yang, and X. G. Peng, "Size control of gold nanocrystals in citrate reduction: The third role of citrate," *J. Amer. Chem. Soc.*, vol. 129, pp. 13939–13948, 2007.
[30] S. J. Park and D. G. Lee, "Performance improvement of micron-sized fibrous metal filters by direct growth of carbon nanotubes," *Carbon*, vol. 44, pp. 1930–1935, 2006.
[31] A. S. Brady-Estevez, S. Kang, and M. Elimelech, "A single-walled-carbonnanotube filter for removal of viral and bacterial pathogens," *Small*, vol. 4, pp. 481–484, 2008.
[32] G. Viswanathan, D. B. Kane, and P. J. Lipowicz, "High efficiency fine particulate filtration using carbon nanotube coatings," *Adv. Mater.*, vol. 16, pp. 2045–2049, 2004.
[33] A. Srivastava, O. N. Srivastava, S. Talapatra, R. Vajtai, and P. M. Ajayan, "Carbon nanotube filters," *Nat. Mater.*, vol. 3, pp. 610–614, 2004.
[34] B. J. Hinds, N. Chopra, T. Rantell, R. Andrews, V. Gavalas, and L. G. Bachas, "Aligned multiwalled carbon nanotube membranes," *Science*, vol. 303, pp. 62–65, 2004.
[35] J. K. Holt, H. G. Park, Y. M. Wang, M. Stadermann, A. B. Artyukhin, C. P. Grigoropoulos, A. Noy, and O. Bakajin, "Fast mass transport through sub-2-nanometer carbon nanotubes," *Science*, vol. 312, pp. 1034–1037, 2006.
[36] X. F. Wang, X. M. Chen, K. Yoon, D. F. Fang, B. S. Hsiao, and B. Chu, "High flux filtration medium based on nanofibrous substrate with hydrophilic nanocomposite coating," *Environ. Sci. Technol.*, vol. 39, pp. 7684–7691, 2005.
[37] M. Yu, H. H. Funke, J. L. Falconer, and R. D. Noble, "High density, vertically-aligned carbon nanotube membranes," *Nano Lett.*, vol. 9, pp. 225–229, 2009.
[38] E. T. Mickelson, C. B. Huffman, A. G. Rinzler, R. E. Smalley, R. H. Hauge, and J. L. Margrave, "Fluorination of single-wall carbon nanotubes," *Chem. Phys. Lett.*, vol. 296, pp. 188–194, 1998.
[39] J. Nelson, *The Physics of Solar Cells*. London, U.K.: Imperial College Press, 2008.
[40] C. Chen, M. C. Plante, C. Fradin, and R. R. LaPierre, "Layer-by-layer and step-flow growth mechanisms in gaasp/gap nanowire heterostructures," *J. Mater. Res.*, vol. 21, pp. 2801–2809, 2006.
[41] D. E. Perea, E. R. Hernesath, E. J. Schwalbach, J. L. Lensch-Falk, P. W. Voorhees, and L. J. Lauhon, "Direct measurement of dopant distribution in an individual vapour-liquid-solid nanowire," *Nat. Nanotechnol.*, vol. 4, pp. 315–319, 2009.
[42] J. E. Allen, D. E. Perea, E. R. Hemesath, and L. J. Lauhon, "Nonuniform nanowire doping profiles revealed by quantitative scanning photocurrent microscopy," *Adv. Mater.*, vol. 21, pp. 1–6, 2009.
[43] O. Gunawan and S. Guha, "Characteristics of vapor-liquid-solid grown silicon nanowire solar cells," *Sol. Energy Mater. Sol. C*, vol. 93, pp. 1388–1393, 2009.
[44] T. Stelzner, M. Pietsch, G. Andra, F. Falk, E. Ose, and S. Christiansen, "Silicon nanowire-based solar cells," *Nanotechnology*, vol. 19, pp. 295203-1–295203-4, 2008.
[45] A. Benham, J. L. Johnson, Y. Choi, M. G. Estosun, O. A. K., P. Kapur, K. C. Saraswat, and A. Ural, "Experimental characterization of single-walled carbon nanotube film-Si Schottky contacts using metal-semiconductor-metal structures," *Appl. Phys. Lett.*, vol. 92, pp. 243116-1–243116-3, 2008.
[46] I. H. Tan, G. L. Snider, L. D. Chang, and E. L. Hu, "A self-consistent solution of Schrodinger-Poisson equations using a nonuniform mesh," *J. Appl. Phys.*, vol. 68, pp. 4071–4076, 1990.
[47] E. Havard, T. Camps, V. Bardinal, L. Salvagnac, C. Armand, C. Fontaine, and S. Pinaud, "Effect of thermal annealing on the electrical properties of indium tin oxide (ITO) contact on Be-doped GaAs for optoelectronic applications," *Semicond. Sci. Technol.*, vol. 23, pp. 035001-1–035001-4, 2008.

Parsian K. Mohseni received the B.Eng. degree in engineering physics in 2005 form McMaster University, Hamilton, ON, Canada, where he is currently working toward the Ph.D. degree, as part of the Nanostructures and Optoelectronics Research Group, under supervision of Dr. Ray LaPierre, in the Department of Engineering Physics.

His current research interests include growth and characterization of semiconductor nanostructures, and the development of nanowire-based optoelectronic devices.

Mr. Mohseni is a member of the Materials Research Society, the American Chemical Society, the Microscopical Society of Canada, and the Society of Photo-Optical Instrumentation Engineers.

Gregor Lawson received the M.Sc. degree in pure and applied chemistry from the University of Strathclyde, Glasgow, U.K., in 2004. He is currently working toward the Ph.D. degree in the Department of Chemistry and Chemical Biology, McMaster University, Hamilton, ON, Canada, working under the supervision of Dr. A. Adronov.

His research interests include the polymer chemistry of carbon nanotubes, synthesis of inorganic nanoparticles, and the development of novel nanostructured composite materials.

Alex Adronov received his B.Sc. degree in chemistry from McMaster University, Hamilton, ON, Canada, in 1996. He then joined graduate studies in the group of Prof. J. M. J. Fréchet at the University of California, Berkeley, where he received his Ph.D. degree in 2001.

He began his independent career as an Assistant Professor at McMaster University in 2001, and was promoted to Associate Professor in 2007. His current research interests include the polymer chemistry of carbon nanotubes, conjugated polymers, and novel polymer architectures for therapeutic applications.

Ray R. LaPierre (M'04) received the B.Sc. degree in physics from Dalhousie University, Halifax, NS, Canada, in 1992, the M.Eng. degree in 1994 and the Ph.D. degree in 1997 from McMaster University, Hamilton, ON, Canada.

He was involved in the development of molecular beam epitaxy techniques. In 1997, he joined JDS Uniphase, Ottawa, ON, as a Research Engineer, where he developed dielectric coatings for application in telecommunications components. In 2004, he rejoined McMaster University as an Assistant Professor in the Engineering Physics Department, where he is currently an Associate Professor and an Associate Chair (Undergraduate) in the Engineering Physics Department. His current research interests include the growth and application of semiconductor nanowires.

Dr. LaPierre is a member of the Professional Engineers Ontario, the Materials Research Society, the Canadian Association of Physicists, and the American Vacuum Society.